Double-network gels with dynamic bonds under multi-cycle deformation

Drozdov, A. D.; Christiansen, Jesper De C.

Published in:
Journal of the Mechanical Behavior of Biomedical Materials

DOI (link to publication from Publisher):
10.1016/j.jmbbm.2018.08.001

Publication date:
2018

Document Version
Accepted author manuscript, peer reviewed version

Citation for published version (APA):
Drozdov, A. D., & Christiansen, J. D. C. (2018). Double-network gels with dynamic bonds under multi-cycle deformation. *Journal of the Mechanical Behavior of Biomedical Materials*, *88*(December 2018), 58-68. https://doi.org/10.1016/j.jmbbm.2018.08.001


www.elsevier.com/locate/jmbbm

Double-network gels with dynamic bonds under multi-cycle deformation

A.D. Drozdov, J. deClaville Christiansen

PII: S1751-6161(18)30693-3
DOI: https://doi.org/10.1016/j.jmbbm.2018.08.001
Reference: JMBBM2912

To appear in: *Journal of the Mechanical Behavior of Biomedical Materials*

Received date: 2 May 2018
Revised date: 14 June 2018
Accepted date: 1 August 2018

Cite this article as: A.D. Drozdov and J. deClaville Christiansen, Double-network gels with dynamic bonds under multi-cycle deformation, *Journal of the Mechanical Behavior of Biomedical Materials,* https://doi.org/10.1016/j.jmbbm.2018.08.001

Double-network gels with dynamic bonds under multi-cycle deformation

A.D. Drozdov* and J. deClaville Christiansen
Department of Materials and Production
Aalborg University
Fibigerstraede 16, Aalborg 9220, Denmark

Abstract

Application of double-network (DN) gels with dynamic bonds as implants for repair of damaged and degenerate cartilage tissue and their use as synthetic non-degradable scaffolds for growth, proliferation and differentiation of stem cells requires understanding of the mechanical behavior of these materials under cyclic deformation. A constitutive model is developed for the viscoelastic and viscoplastic responses of DN gels with covalent and non-covalent junctions under multi-cycle loading. Viscoelasticity is treated as breakage and reformation of temporary junctions driven by thermal fluctuations. Viscoplasticity is thought of as sliding of permanent junctions with respect to their initial positions in the polymer network. Adjustable parameters in the governing equations are found by fitting observations in tensile loading–unloading tests with various maximum strains and multi-cycle tests with monotonically increasing maximum elongation ratios per cycle on two DN gels with physical junctions formed due to hydrogen bonds and ionic complexation. Numerical analysis demonstrates the ability of the model not only to describe observations correctly, but also to predict the mechanical response in multi-cycle tests with sophisticated deformation programs. Quantitative and qualitative effects of metal-coordination bonds on the mechanical behavior of supramolecular gels are revealed by simulation.

Key-words: Double-network gel; Dynamic bonds; Cyclic deformation; Mullins effect; Fatigue

1 Introduction

Hydrogels are “soft and wet” materials formed by water-swollen three-dimensional networks of hydrophilic chains bridged by covalent and non-covalent bonds (Osada and Gong, 1998). Mechanical

---

*E–mail: aleksey@mp.aau.dk

and physical properties of hydrogels resemble those of soft biological tissues, which makes them suitable for a wide range of potential applications in regenerative medicine (Annabi et al., 2014), tissue engineering (Leijten et al., 2017), bioprinting of stem cells (Leberfinger et al., 2017), living tissues and artificial organs (Mandrycky et al., 2016), targeted drug delivery (Li and Mooney, 2016), biosensing (Peppas and Van Blarcom, 2016), as well as manufacturing of implantable devices (Chin et al., 2017) and actificial muscles (Ko and Javey, 2017).

Conventional gels with polymer chains bridged by covalent cross-links are relatively weak and brittle (Tanaka et al., 2005), which restricts the area of their biomedical applications as these materials cannot be employed in regeneration of load-bearing tissues. This shortcoming of chemically cross-linked gels is explained by inhomogeneity of their polymer networks, weak interactions between chains, and the lack of an efficient mechanism for energy dissipation (Gong, 2014).

Strength and toughness of a gel can be enhanced noticeably by formation of a double-network (DN) structure that involves two or more inter-penetrating networks of chains (Gong, 2014). The most promising strategy to prepare polymer networks with superior mechanical properties consists in introduction of sacrificial (dynamic) bonds between chains governed by reversible interactions (Wojtecki et al., 2011). Design of DN gels with covalent and non-covalent bonds that demonstrate high stiffness, strength, toughness, and fatigue resistance has recently become a focus of attention (Zhao, 2014; Chen et al., 2016; Creton, 2017). The following mechanisms have been proposed for the development of dynamic bonds in a polymer network (Wang et al., 2017; Mann et al., 2018): (i) electrostatic interaction (formation of polyion complexes), (ii) metal-ligand coordination, (iii) hydrophobic association, (iv) hydrogen bonding, (v) host-guest recognition, and (vi) reinforcement with nanoparticles.

The response of a gel with permanent (covalent) junctions between chains is merely elastic. When temporary (physical) bonds are introduced in a network, its behavior becomes time- and rate-dependent (Rose et al., 2013; Hu et al., 2017). These features can be described within the concept of transient networks where chains with sticky ends detach from and attach to temporary junctions being driven by thermal fluctuations (Green and Tobolsky, 1946; Tanaka and Edwards, 1992). The viscoelastic phenomena in a DN gel are accompanied by the viscoplastic effects (Meng et al., 2016) that reflect slippage of junctions with respect to their initial positions in the network (Drozdov, 2010).

This study focuses on the viscoelastic and viscoplastic responses of DN gels with covalent and non-covalent bonds observed under cyclic loading with various deformation programs. Our interest to the analysis of multi-cycle deformation is driven by the following biomedical applications:

(I) Implantation of DN gels for (i) reinforcement of weakened regions in osteoartritic articular cartilage (Cooper et al., 2016), (ii) repair of osteochondral defects in damaged cartilage (Kitamura et al., 2016), (iii) total meniscus replacement (Rey-Rico et al., 2017; Fischenich et al., 2018), and (iv) replacement of the nucleus pulposus (inner core) in degenerated intervertebral discs (Perez-San Vicente et al., 2017; Frauchiger et al., 2017). Cyclic loading of the implants is induced by motion (walking and running) of humans and animals, while the viscoelastic and viscoplastic dissipation of energy by DN gels allows them to serve as shock absorbers for the damaged tissue.

(II) Three-dimensional hydrogel scaffolds for growth, migration, proliferation and differentiation of stem cells are conventionally prepared from (a) biological molecules bridged by physical bonds and (b) synthetic chains connected by covalent junctions. In the latter case, biodegradation of the polymer network is essential to make room for the new tissue produced by cells (Dhote and Vernerey, 2014; Liu et al., 2018). Development of non-degradable synthetic scaffolds where polymer chains are bridged by dynamic bonds, and growth of cells is not restricted by permanent junctions has recently attracted substantial attention (Yang et al., 2017; Zhao et al., 2018; Yu et al, 2018; Zhai et al., 2018), see (Zhou et al., 2017) for review. In cell-laden gels, cells sense the scaffold properties, integrate external cues, and translate the signaling information into the cell fate decision and lineage specification (Hao et al., 2015; Yang et al., 2017). Observation (Dan et al., 2015; Vining and Mooney, 2017) show that differentiation of stem cells can be accelerated noticeably by cyclic deformation (mechanical cue). In particular, the rates of stem cell differentiation and tissue formation are affected strongly by periodic loading under uniaxial (Song et al., 2018) and biaxial (Cao et al., 2018) tension, compression (Brunelli et al., 2017) and shear (Liu et al., 2015), and they are influenced noticeably by stress relaxation under rest between intervals of excitations (Chaudhuri et al., 2016; Charrier et al., 2018).

The objective of this work is threefold: (i) to develop a model for DN gels that accounts for their viscoelastic and viscoplastic responses under multi-cycle deformation and to determine adjustable parameters in the governing equations by fitting experimental stress–strain diagrams, (ii) to demonstrate the ability of the constitutive relations to predict observations in cyclic tests with various (strain-controlled, stress-controlled and mixed) deformation programs and arbitrary stresses (strains) at which transitions from stretching to retraction and from unloading to reloading occur, and (iii) to apply the model for comparison of two supramolecular gels with the same polymer chains but different types of physical bonds between them.

A constitutive framework for the description of the viscoelastic behavior of polymer networks with permanent and temporary junctions was developed in (Long et al., 2014; Guo et al., 2016; Li et al., 2016; Wang and Gao, 2016; Vernerey et al., 2017; Drozdov, 2017; Mao et al., 2017; Vernerey, 2018; Zhou et al., 2018). Constitutive equations for the viscoelastic and viscoplastic behavior of

DN gels under cyclic loading have recently been derived in (Tang et al., 2016; Liu et al., 2016; Lu et al., 2017; Bacca et al., 2017; Drozdov and deClaville Christiansen, 2018).

The novelty of our approach consists in (i) the description of both phenomena (viscoelasticity and viscoplasticity) within a unified constitutive model grounded on the free energy imbalance inequality, and (ii) the account for two mechanisms of plastic flow induced by macro-deformation and inter-chain interaction.

An equivalent polymer network in a DN gel is treated as a combination of two networks: chains in the permanent network are linked by covalent cross-links, while chains in the transient network are bridged by temporary junctions. The viscoelastic response of the gel reflects breakage and reformation of temporary bonds (transition of chains connected by physical junctions from their active to dangling state and vice versa). The transient network is presumed to be inhomogeneous and composed of meso-regions with various activation energies for rearrangement (Drozdov and Gupta, 2003; Drozdov and Yuan, 2003). This allows the entire relaxation spectrum to be described in terms of the distribution function for these meso-regions.

The viscoplastic behavior of a DN gel reflects slippage of junctions in the permanent network with respect to their reference positions. A junction between chains becomes unbalanced when one of the chains connected by this junction is transformed from the active state into the dangling state. As a result, the junction begins to slide with respect to the network (viscoplastic flow) until it reaches a new equilibrium state (Filippidi et al., 2017). Two mechanisms of plastic deformation are taken into account: (i) when junctions slide with respect to their initial positions with the rate proportional to the strain rate, and (ii) when the rate of sliding of junctions is governed by the energy of inter-chain interaction (Drozdov et al., 2013).

2 Model

A gel is treated as a two-phase medium composed of an equivalent polymer network and water molecules. The solid and fluid phases are modeled as immiscible interpenetrating continua. Deformation of the network and concentration of water molecules are connected by the molecular incompressibility condition.

The polymer network in a DN gel is thought of as a superposition of two networks. Chains in the permanent network are linked by permanent junctions, while chains in the transient network are bridged by temporary bonds that rearrange (break and reform) being driven by thermal fluctuations. According to the affinity hypothesis, deformations of the permanent and transient networks coincide with macro-deformation of the gel.

The reference (stress-free) state of the permanent network before application of external loads coincides with the as-prepared state of the gel. According to the multiplicative decomposition formula, the deformation gradient $\mathbf{F}$ for transition from the initial (undeformed dry) state into the actual (deformed swollen) state is given by $\mathbf{F} = \mathbf{F}_{\rm e} \cdot \mathbf{F}_{\rm p}$, where $\mathbf{F}_{\rm e}$ and $\mathbf{F}_{\rm p}$ are the deformation gradients for elastic and plastic deformations, and the dot stands for inner product.

Two mechanisms of plastic deformation (sliding of junctions between chains with respect to their initial positions) are introduced: (i) induced by macro-deformation and (ii) driven by inter-chain interaction. In the unloaded state, the rate-of-strain tensors for the corresponding plastic flows read $\mathbf{d}_{\rm m}$ and $\mathbf{d}_{\rm i}$, respectively. The rate-of-strain tensor for the entire plastic deformation is determined by $\mathbf{d}_{\rm p} = \mathbf{d}_{\rm m} + \mathbf{d}_{\rm i}$ (for definition of these tensors, see Eqs. (S-6) to (S-15) in Supplementary Material).

The rate-of-strain tensor $\mathbf{D}_{\rm m}$ (an analog of $\mathbf{d}_{\rm m}$ in the actual state) is proportional to the rate-of-strain tensor for macro-deformation $\mathbf{D}_{\rm m} = \phi \mathbf{D}$. The non-negative coefficient ϕ vanishes in the initial state (the corresponding plastic flow is negligible at infinitesimal strains), increases under deformation (which accelerates the sliding process), and tends to its ultimate value (that corresponds to the developed plastic flow) at large strains. Evolution of the function ϕ is governed by the phenomenological equation

$$\dot{\phi} = \pm A (1 - \phi)^2, \qquad \phi(0) = 0, \tag{1}$$

where the superscript dot stands for the derivative with respect to time, and the signs "+" and "−" correspond to loading and unloading, respectively. The coefficient A reads

$$A = a (I_1 - 2)^{-\frac{3}{2}}, \tag{2}$$

where a is a positive adjustable parameter, and I_1 is the first principal invariant of the Cauchy–Green tensor for macro-deformation. Under uniaxial tension with elongation ratio λ, the presence of $I_1 = \lambda^2 + 2/\lambda$ in Eq. (2) ensures that ϕ reaches a constant value at large elongation ratios.

To describe the response of a transient network, we denote by τ an instant when an active chain (both ends are connected to the network) is bridged with the network by a temporary junction, and distinguish chains that joined the network under polymerization of a pre-gel solution ($\tau = 0$) and those attaching the network under deformation ($\tau > 0$). The reference (stress-free) state of a chain with $\tau = 0$ coincides with the as-prepared state of the gel. The reference state of a chain with $\tau > 0$ coincides with the actual state of the gel at instant τ (stresses in chains totally relax under rearrangement).

The transient network is presumed to be inhomogeneous and composited of meso-domains with various activation energies U for breakage of dynamic bonds. The non-homogeneity is described by the distribution function $f(u)$ of meso-domains with dimensionless activation energies $u = U/(k_{\rm B}T)$, where k_{B} is the Boltzmann constant, and T stands for the absolute temperature. The quasi-Gaussian expression is adopted for this function

$$f(u) = f_0 \exp\Bigl(-\frac{u^2}{2\Sigma^2}\Bigr) \qquad (u \geq 0), \tag{3}$$

where $\Sigma > 0$ is a material constant, and the coefficient f_0 is determined from the normalization condition $\int_0^\infty f(u)\mathrm{d}u = 1$. Rearrangement of the inhomogeneous network is entirely determined by the rate of detachment of active chains from temporary junctions (Meng et al., 2016)

$$\Gamma = \gamma_* \exp(-u) \tag{4}$$

with

$$\gamma_* = \gamma \exp\Bigl[-\alpha(I_{\mathrm{i}2} - 3)\Bigr]. \tag{5}$$

Here γ is the attempt rate for rupture of dynamic bonds at infinitesimal strains, the exponent α describes slowing down of the rearrangement process driven by plastic deformation, and $I_{\mathrm{i}2}$ is the second principal invariant of the Cauchy–Green tensor $\mathbf{B}_{\mathrm{i}} = \mathbf{F}_{\mathrm{i}} \cdot \mathbf{F}_{\mathrm{i}}^{\top}$, where $\top$ denotes transpose. Eq. (5) describes mechanically-induced changes in the rate of separation of chains from temporary junctions. This relation is in accord with experimental data reported in (Nishida et al., 2012; Lu et al., 2017), to mention a few.

Constitutive equations for the mechanical response of a DN gel under an arbitrary deformation with finite strains are developed in Appendix A (Supplementary Material). These relations are derived by means of the free energy imbalance inequality for an arbitrary specific mechanical energy of the permanent network $W_{\mathrm{e}}(I_{\mathrm{e}1}, I_{\mathrm{e}2}, I_{\mathrm{e}3}) + W_{\mathrm{i}}(I_{\mathrm{i}1}, I_{\mathrm{i}2})$ and an arbitrary strain energy per chain in the transient network $w(I_{\tau 1}, I_{\tau 2}, I_{\tau 3})$. The energy W_{e} stored in chains of the permanent network depends on the principal invariants $I_{\mathrm{e}m}$ of the Cauchy–Green tensor for elastic deformation $\mathbf{B}_{\mathrm{e}} = \mathbf{F}_{\mathrm{e}} \cdot \mathbf{F}_{\mathrm{e}}^{\top}$. The energy of inter-chain interaction W_{i} is treated as a function of the principal invariants $I_{\mathrm{i}m}$ of the Cauchy–Green tensor for plastic deformation $\mathbf{B}_{\mathrm{i}}$. The energy w stored in an active chain depends on the principal invariants $I_{\tau m}$ of the Cauchy–Green tensor $\mathbf{b}_{\tau} = \mathbf{f}_{\tau} \cdot \mathbf{f}_{\tau}^{\top}$, where $\mathbf{f}_{\tau}(t) = \mathbf{F}(t) \cdot \mathbf{F}^{-1}(\tau)$ denotes the deformation gradient for transition from the actual state at time τ to the actual state at time t.

In the analysis of observations, we focus on uniaxial cyclic tension of a DN gel with the strain energy density of the permanent network (Gent, 1996)

$$W_{\mathrm{e}} = -\frac{1}{2} G_{\mathrm{e}} \Bigl[K \ln\Bigl(1 - \frac{I_{\mathrm{e}1} - 3}{K}\Bigr) + \ln I_{\mathrm{e}3}\Bigr], \tag{6}$$

the energy of inter-chain interactions

$$W_{\mathrm{i}} = \frac{1}{2} G_{\mathrm{i}} (I_{\mathrm{i}1} - 3), \tag{7}$$

and the energy of active chains in the transient network

$$w = \frac{1}{2} g \Big[(I_{\tau 1} - 3) - \ln I_{\tau 3} \Big], \tag{8}$$

where $G_{\rm e}$, $G_{\rm i}$, g and K are constants. Eq. (6) for the function $W_{\rm e}$ provides a simplified version of the eight-chain model (Bergstrom and Boyce, 1998) that allows strain-hardening of DN gels to be accounted at large elongation ratios (Luo et al., 2016). The neo-Hookean expression (7) for $W_{\rm i}$ serves as the first term in the formal expansion of the function $W_{\rm i}$ into the Taylor series with respect to its arguments. Eq. (8) was developed in (Drozdov, 2014) within the concept of entropic elasticity.

The governing equations for a DN gel equilibrated before loading and subjected to uniaxial tensile cyclic deformation with a constant strain rate $\dot{\epsilon}$ involve

(i) the formula for engineering tensile stress (see Eq. (S-83) in Supplementary Material)

$$\sigma = G \Big[(1-\kappa)(1-\phi) V \frac{\lambda_{\rm e}^3 - 1}{\lambda \lambda_{\rm e}} + \kappa \Big(S_1 \lambda - \frac{S_2}{\lambda^2} \Big) \Big], \tag{9}$$

where

$$V = \Big[1 - \frac{1}{K} \Big(\lambda_{\rm e}^2 + \frac{2}{\lambda_{\rm e}} - 3 \Big) \Big]^{-1},$$

(ii) the kinematic equation for elongation ratio λ under macro-deformation

$$\dot{\lambda} = \pm \dot{\epsilon}, \qquad \lambda(0) = 1, \tag{10}$$

(iii) the kinematic equation for elongation ratio $\lambda_{\rm e}$ for elastic deformation (this relation follows from Eqs. (S-75) and (S-77))

$$\frac{\dot{\lambda}_{\rm e}}{\lambda_{\rm e}} = (1-\phi) \frac{\dot{\lambda}}{\lambda} - \frac{\dot{\lambda}_{\rm i}}{\lambda_{\rm i}}, \qquad \lambda_{\rm e}(0) = 1, \tag{11}$$

(iv) the kinetic equation (S-77) for elongation ratio $\lambda_{\rm i}$ under plastic deformation

$$\frac{\dot{\lambda}_{\rm i}}{\lambda_{\rm i}} = P \Big(V \frac{\lambda_{\rm e}^3 - 1}{\lambda_{\rm e}} - R \frac{\lambda_{\rm i}^3 - 1}{\lambda_{\rm i}} \Big), \qquad \lambda_{\rm i}(0) = 1, \tag{12}$$

(v) the integral relations for functions S_1 and S_2 defined by Eq. (S-81)

$$S_1 = \int_0^\infty f(u) s_1(t,u) {\rm d}u, \qquad S_2 = \int_0^\infty f(u) s_2(t,u) {\rm d}u, \tag{13}$$

(vi) the kinetic equations (S-79) for functions s_1 and s_2

$$\frac{\partial s_1}{\partial t} = \Gamma \Big(\frac{1}{\lambda^2} - s_1 \Big), \qquad \frac{\partial s_2}{\partial t} = \Gamma (\lambda - s_2), \qquad s_1(0,u) = s_2(0,u) = 1. \tag{14}$$

Eqs. (9)–(14) together with Eqs. (1)–(5) involve six material constants: G stands for the elastic modulus of a gel, K^{-1} is the Gent constant, κ denotes the ratio of elastic moduli of transient and permanent networks, a characterizes plastic flow of junctions induced by macro-deformation, γ is the attempt rate for breakage of dynamic bonds, and Σ is a measure of inhomogeneity of the transient network.

Three regimes are distinguished in the analysis of multi-cycle deformation: (i) stretching of a virgin sample ($\dot{\lambda} > 0$), (ii) retraction ($\dot{\lambda} < 0$), and (iii) reloading ($\dot{\lambda} > 0$). The constitutive equations contain three adjustable functions: P, R and α. These functions are presumed to be governed by different laws under stretching, retraction and reloading.

The coefficient P characterizes the rate of sliding of junctions driven by inter-chain interaction. This parameter vanishes under stretching and accepts different values, P_1 and P_2, under retraction and reloading:

$$P = 0 \quad \text{(stretching)}, \qquad P = P_1 \quad \text{(retraction)}, \qquad P = P_2 \quad \text{(reloading)}. \tag{15}$$

The rate of plastic flow along each retraction path is constant,

$$P_1 = P_{1*}, \tag{16}$$

where P_{1*} denotes the rate of sliding of junctions at the instant when unloading starts. The rate of plastic flow along each reloading path reads

$$P_2 = P_{2*} \exp\Big[\beta(\sigma - \sigma_{\rm min})\Big], \tag{17}$$

where P_{2*} is the rate of sliding of junctions at the instant when retraction starts and tensile stress equals its minimum value $\sigma_{\rm min}$, and the coefficient β describes stress-induced acceleration of the slippage process under reloading. The quantities P_{1*} and P_{2*} evolve with elongation ratios $\lambda_{\rm max}$ and $\lambda_{\rm min}$ at which unloading and reloading occur. Changes in P_{1*} and P_{2*} with $\lambda_{\rm max}$ and $\lambda_{\rm min}$ are described by the phenomenological relations

$$\log P_{1*} = P^0_{1*} + P^1_{1*}(I_{\rm e2} - 3), \qquad \log P_{2*} = P^0_{2*} + P^1_{2*}(I_{\rm i2} - 3), \tag{18}$$

where $\log = \log_{10}$, and the principal invariants of the Cauchy–Green tensors for elastic $I_{\rm e2} = 2\lambda_{\rm e} + \lambda_{\rm e}^{-2}$ and plastic $I_{\rm i2} = 2\lambda_{\rm i} + \lambda_{\rm i}^{-2}$ deformations are calculated at the points where the strain rate $\dot{\epsilon}$ changes its sign. Eq. (18) reflects damage accumulation (changes in the micro-structure of DN gels) under multi-cycle deformation.

The parameter R denotes the ratio of moduli $G_{\rm i}$ and $G_{\rm e}$ that characterize mechanical energies dissipated by and stored in the permanent network. By analogy with Eq. (15), we presume this quantity to accept different values under retraction and reloading

$$R = R_1 \quad \text{(retraction)}, \qquad R = R_2 \quad \text{(reloading)}, \tag{19}$$

where R_1 and R_2 are constants independent of elongation ratios $\lambda_{\rm max}$ and $\lambda_{\rm min}$ at which unloading and reloading start.

The exponent α accounts for the effect of plastic deformation on rearrangement of temporary junctions. Along each cycle of loading–unloading, this quantity accepts a fixed value. This value is affected, however, by the maximum elongation ratio $\lambda_{\rm max}$ at the instant when retraction starts. The dependence of α on $\lambda_{\rm max}$ is described by the equation similar to Eq. (18),

$$\log\alpha = \alpha^0 + \alpha^1(I_{\rm e2} - 3), \qquad (20)$$

where $I_{\rm e2}$ is evaluated at the elongation ratio $\lambda = \lambda_{\rm max}$. Eq. (20) reflects the effect of mechanical factors on the rates of rupture and reformation of physical bonds (Cui et al., 2016).

To ensure the ability of the model to describe experimental stress–strain diagrams on DN gels under multi-cycle deformation with an arbitrary program (variable elongation ratios $\lambda_{\rm max}$ and $\lambda_{\rm min}$ at which the strain rate changes its sign), mutual dependencies are introduced between the rate of plastic flow and stresses (Eq. (17)) and between elastic, viscoelastic and viscoplastic responses (Eqs. (5), (18) and (20)). Although these dependencies lead to an increase in the number of material constants, the total number of adjustable parameters in the governing equations remains lower than that in other models for the viscoelastic and viscoplastic responses of polymers under cyclic deformation.

3 Fitting of observations

The constitutive model is applied to fit experimental stress–strain diagrams on two acrylamide–acrylic acid–*N*-butyl methacrylate (AAm-AAc-BMA) copolymer gels in cyclic tests with various deformation programs.

The gels were synthesized with the help of a three-stage procedure (Liang et al., 2017). At the first stage, core-shell microgel particles were prepared by micellar copolymerization (6 h at 70 °C) of AAm monomers (0.185 g, 3.2 mmol) and hydrophobic BMA monomers (2.135 g, 16.3 mmol) in an aqueous solution of ionic surfactant sodium dodecyl sulfate (SDS, 0.0375 g, 0.14 mmol) by using N,N'-methylene-bis-acrylamide (BIS, 0.0305 g, 0.20 mmol) as a cross-linker and ammonium persulfate (APS, 2.94 g of 1.5 wt% aqueous solution at 0.19 mmol) as an initiator.

At the other stage, a DN gel was manufactured by free radical polymerization (24 h at 25 °C) of AAm and AAc monomers (15 wt.%, molar ratio of AAm and AAc equals 97:3) and the microgel particles (20 wt.% of monomers) in an aqueous solution with pH=3 by using APS as an initiator. This gel is denoted as H-gel ("H" stands for hydrogen bonds between polymer chains and water molecules).

At the final stage, samples were immersed (30 min at room temperature) in an aqueous solution of iron chloride hexahydrate $\mathrm{FeCl_3 \cdot 6H_2O}$ (50 mM) for ionic complexation. The obtained gel is designated as IH-gel ("I" stands for ionic complexes between mobile $\mathrm{Fe^{3+}}$ cations and ionized carboxyl group).

The dual-network structures in H-gel and IH-gel are formed by permanent cross-links of AAm–AAc chains with microgel particles and their physical cross-links with hydrogen bonds and ionic complexes.

Mechanical tests were conducted at room temperature on as-prepared specimens with degree of swelling $Q_0 = 3.2$ (this parameter remains practically unaffected by soaking of samples in $\mathrm{FeCl_3}$ solution). The experimental program involved: (i) loading–unloading tests with strain rate $\dot{\epsilon} = 0.0083$ s^{-1} and various maximum elongation ratios $\lambda_{\max}$ ranging from 1.5 to 4.0, and (ii) multi-cycle tests ($N = 4$) in which sample were stretched with the same strain rate $\dot{\epsilon}$ up to the elongation ratios $\lambda_{\max 1} = 1.5$, $\lambda_{\max 2} = 2.0$, $\lambda_{\max 3} = 3.0$, $\lambda_{\max 4} = 4.0$ and unloaded down to the zero stress.

Figure 1.

Experimental data in the loading–unloading tests with various $\lambda_{\max}$ are depicted in Fig. 1. Bearing in mind that observations on the time-dependent response were not provided, we determine the constants γ, Σ and κ together with G, a and K from the best-fit conditions for the loading paths of the stress–strain diagrams with $\lambda_{\max} = 4.0$. When experimental data in relaxation tests are available, γ, Σ and κ can be determined separately by matching the relaxation curves. Afterwards, P_{1*}, R_1 and α are found by fitting observations under retraction in the tests with $\lambda_{\max} = 4.0$. Finally, we fix R_1 and approximate experimental data under unloading in tests with other $\lambda_{\max}$ by means of two parameters, P_{1*} and α. Evolution of these quantities with maximum elongation ratio $\lambda_{\max}$ is illustrated in Fig. 2, where the data are approximated by Eqs. (18) and (20).

Figure 2.

The values of material constants are collected in Tab. 1.

Table 1.

Fig. 1 demonstrates that the presence of ionic bonds affects strongly the response of DN gels in cyclic tests. In particular,

(I) Ionic complexation results in a pronounced increase in tensile stresses under tension: σ at $\lambda = 4$ in IH-gel exceeds that in H-gel by a factor of 4.7. This is reflected in the model by two factors: (a) the elastic modulus G of IH-gel is higher than that for H-gel by 40%, and (b) the coefficient a (describing plastic flow under stretching) adopts a relatively high value for H-gel and vanishes for IH-gel.

(II) Formation of ionic complexes induces changes in the shape of stress–strain diagrams that become substantially less curved. This observation is accounted for in the model by a decay in parameter a (responsible for the viscoplastic response) and a strong (by a factor of 5) increase in Σ (which characterizes the viscoelastic behavior).

(III) Development of ionic bonds leads to a reduction in residual strain (elongation ratio $\lambda_{\min}$ at the instant when tensile stress vanishes at retraction). This fact is reflected by a substantial increase in R_1 and decrease in α for IH-gel compared with H-gel.

Figure 3.

We proceed with matching observations in multi-cycle tests with monotonically increasing maximum elongation ratios $\lambda_{\max n}$ depicted in Fig. 3 (for clarity, data along each cycle of loading–unloading are reported in a separate panel). In the deformation program chosen in (Liang et al., 2017), retraction of samples is conducted down to the zero strain (not zero stress). As a result, the stress–strain diagrams involve intervals with negative (compressive) stresses. Under compression, the samples are buckled (Long et al., 2014), which results in damage accumulation in the gels. In the fitting procedure, we presume retraction to be performed down to the zero stress, determine adjustable parameters, and assess the effect of damage growth by comparing parameters found in approximation of experimental data in Figs. 1 and 3.

Keeping in mind that observations along the first loading path in Fig. 3 deviate slightly from those in Fig. 1, we approximate these data separately. The algorithm of matching observations is similar to that applied to fit the data in Fig. 1. The coefficients G, a, K and κ are determined by matching the envelope of the loading paths (to reduce the number of adjustable parameters, the same values of γ and Σ are used as in Fig. 1). Each retraction path in Fig. 3 is fitted by means of two parameters, P_{1*} and α (the value of R_1 is taken from Tab. 1). The first reloading path is approximated with the help of three parameters, P_{2*}, R_2 and β. Then the quantities R_2 and β are fixed, and each remaining reloading path is fitted by means of the only coefficient P_{2*}. The best-fit values of material constants are listed in Tab. 2. Tabs. 1 and 2 show that adjustable parameters adopt similar values, which implies that our algorithm of fitting observations is stable.

Figure 4.

Evolution of P_{1*} and α with maximum elongation ratio $\lambda_{\max}$ is illustrated in Fig. 4, where the data are approximated by Eqs. (18) and (20). Comparison of Figs. 2 and 4 reveals that extra damage caused by buckling of samples under multi-cycle deformation strengthens the effect of $\lambda_{\rm max}$ on P_{1*} and α (the coefficient $|P^1_{1*}|$ increases from 0.151 to 0.241 for IH-gel, while the coefficient α^1 grows from 0.119 to 0.192 for H-gel), which confirms that Eqs. (18) and (20) describe changes in these parameters induced by damage accumulation.

Figure 5.

The influence of minimum elongation ratio $\lambda_{\rm min}$ (at the point where the strain rate changes its sign) on P_{2*} is shown in Fig. 5, where the data are matched by Eq. (18). This figure demonstrates that the presence of ionic bonds does not affect the rate of decay in P_{2*} with $\lambda_{\rm min}$ (the coefficient P^1_{2*} adopts similar values -6.35 and -6.53 for IH-gel and H-gel). Plastic recovery under reloading is, however, strongly affected by metal coordination bonds: the values of P_{2*} for IH-gel exceed those for H-gel by twice.

The following conclusions are drawn from Figs. 1–5:

(I) The model ensures good agreement between results of simulation and observations in cyclic tests with various $\lambda_{\rm max}$ and multi-cycle tests with monotonically increasing $\lambda_{{\rm max}\,n}$ (Figs. 1 and 3).

(II) Eqs. (18) and (20) describe adequately evolution of adjustable parameters with elongation ratios $\lambda_{\rm max}$ and $\lambda_{\rm min}$ at which the strain rate changes its sign (Figs. 2, 4 and 5).

(III) Formation of ionic bonds between mobile cations and fixed anions leads to the growth of inhomogeneity of the polymer network (Σ), an increase in elastic modulus (G), pronounced slowing down of non-dissipative sliding of junctions under first loading (a), and acceleration of dissipative plastic flow under retraction (P_{1*}) and reloading (P_{2*}).

4 Numerical simulation

To demonstrate the ability of the model to describe observations in multi-cycle tensile tests with various deformation programs and to examine the effect of ionic bonds on the mechanical behavior of DN gels under fatigue conditions, simulation is performed of the governing equations with adjustable parameters collected in Tab. 1 and reported in Figs. 2 and 5.

Figure 6.

We begin with the mechanical response of IH-gel and H-gel in multi-cycle tests with strain rate $\dot{\epsilon} = 0.0083$ s^{-1}, monotonically increasing maximum elongation ratios under stretching $\lambda_{{\rm max}\,n}$ and the zero minimum stress under retraction $\sigma_{\rm min} = 0$. The following deformation programs are studied:

$$N = 3, \qquad \lambda_{\max n} = 1 + n, \tag{21}$$

$$N = 6, \qquad \lambda_{\max n} = 1 + \frac{1}{2}n. \tag{22}$$

Results of numerical analysis are reported in Fig. 6, where the stress–strain diagrams are depicted under uniaxial tension and cyclic loading. This figure demonstrates all characteristic features of the Mullins phenomenon (Diani et al., 2009) in DN gels: (i) at each cycle of deformation, the loading and retraction paths differ substantially (stress softening), (ii) under reloading along the $(n + 1)$th cycle, the stress–strain diagram coincides with that under uniaxial tension, provided that the elongation ratio λ exceeds the maximum elongation ratio $\lambda_{\max n}$ at the nth cycle (the Mullins effect), (iii) the retraction paths coincide for different deformation programs, provided that unloading starts at the same elongation ratio $\lambda_{\max}$ (fading memory of deformation history).

Slight deviations from the Mullins effect in Fig. 6 are worth to be mentioning (the stress under tension exceeds that under cyclic loading). This can be explained by viscoelasticity of DN gels (rearrangement of dynamic bonds at each cycle of loading–retraction). This effect is more pronounced for IH-gel (where breakage and reformation of physical junctions are independent of mechanical factors, $\alpha = 0$) than for H-gel (where this process is decelerated by plastic flow, $\alpha > 0$).

We proceed with the numerical analysis of the mechanical response in multi-cycle tests ($N = 30$) with the fixed strain rate $\dot{\epsilon}$, fixed maximum elongation ratios per cycle $\lambda_{\max}$, and the minimum stress per cycle $\sigma_{\min} = 0$. Results of simulation are reported in Figs. 7 and 8.

Figure 7.

The stress–strain diagrams for $\lambda_{\max} = 2$, 3 and 4 are presented in Fig. 7, which shows that the maximum stress per cycle $\sigma_{\max}$ decreases, and the minimum elongation ratio per cycle $\lambda_{\min}$ increases with number of cycles n. The rates of changes in these quantities grow monotonically with $\lambda_{\max}$.

Figure 8.

The decay in $\sigma_{\max}$ with n is illustrated in Fig. 8. For each $\lambda_{\max}$, the graph $\sigma_{\max}(n)$ can be split into two intervals. The stress $\sigma_{\max}$ is reduced exponentially with n along the first interval. Along the other interval, the maximum stress per cycle decreases linearly with n (Fig. 8A) or becomes independent of n (Fig. 8B). The former type of response was observed in (Zhang et al., 2012), while the latter type was reported in (Tang et al., 2017).

Fig. 8 shows that the duration of the first interval is independent of $\lambda_{\max}$ for IH-gel, and it increases strongly with $\lambda_{\max}$ for H-gel. This difference may be associated with the absence of non-dissipative plastic flow in IH-gel ($a = 0$) and its presence in H-gel ($a > 0$).

Finally, we focus on the behavior of DN gels in low-cycle fatigue tests (Bai et al., 2017; Zhang et al., 2018). Hydrogel samples are subjected to multi-cycle deformation ($N = 30$) with strain rate $\dot{\epsilon} = 0.0083$ s^{-1}, fixed maximum tensile stresses per cycle $\sigma_{\max}$, and the minimum stress per cycle $\sigma_{\min} = 0$. Results of simulation with $\sigma_{\max}$ belonging to the interval between 40 and 80 kPa for IH-gel and ranging from 18 to 22 kPa for H-gel are reported in Figs. 9 (where the stress–strain diagrams are presented) and 10 (where the maximum elongation ratio per cycle $\lambda_{\max}$ is plotted versus number of cycles).

Figure 9.

Fig. 9 demonstrates that the maximum elongation ratio per cycle $\lambda_{\max}$ and the minimum elongation ratio per cycle $\lambda_{\min}$ increase with number of cycles n. The growth of $\lambda_{\max}$ is accelerated strongly by $\sigma_{\max}$, whereas that of $\lambda_{\min}$ is weakly affected by maximum stress per cycle.

Figure 10.

Fig. 10 shows that for each $\sigma_{\max}$, the graph $\lambda_{\max}(n)$ for IH-gel can be split into two parts: $\lambda_{\max}$ grows sub-linearly with n along the first interval (primary fatigue) and increases linearly with number of cycles along the other interval (secondary fatigue). The same pattern is observed for H-gel in a test with relatively small maximum stress per cycle $\sigma_{\max} = 18$ kPa. The situation changes drastically when maximum stress per cycle reaches the value $\sigma_{\max} = 22$ kPa. At this stress, numerical analysis reveals transition from secondary fatigue to tertiary fatigue (catastrophic failure) after 25 cycles of loading.

The following conclusions are drawn from Figs. 6–10:

(I) The model can predict adequately the mechanical response of DN gels under multi-cycle tensile loading with various deformation programs. Results of simulation for cyclic tests with fixed maximum elongation ratios $\lambda_{\max}$, monotonically increasing $\lambda_{\max\,n}$, and fixed maximum stresses $\sigma_{\max}$ are in qualitative agreement with available observations.

(II) Metal-coordination bonds not only affect the stress–strain diagrams quantitatively, but demonstrate the ability to resist fatigue of DN gels and to prevent their fatigue failure.

5 Conclusions

Constitutive equations are derived for the viscoelastic and viscoplastic behavior of DN gels with dynamic bonds. The solid phase of a gel is treated as a combination of two polymer networks: chains are bridged by permanent cross-links in the first network and by temporary junctions the other. The viscoelastic response of a DN gel reflects breakage and reformation of temporary bonds in the transient network. The viscoplastic behavior reflects slippage of junctions in the permanent network with respect to their reference positions. The characteristic feature of the model is the presence of two mechanisms for plastic deformation: (i) non-dissipative, when junctions slide with respect to their initial positions with the rate proportional to the strain rate, and (ii) dissipative with the rate of sliding depending on the energy of inter-chain interaction. The kinetics of dissipative plastic flow under cyclic deformation is governed by differential equations with coefficients adopting different values under the first loading, retraction and reloading.

The model is applied to fit experimental data in tensile loading–unloading tests with various (but fixed) maximum elongation ratios and multi-cycle tests with monotonically increasing maximum strains on two supramolecular gels. In the first, chains are covalently cross-linked by microgel particles and non-covalently bridged by hydrogen bonds. In the other, additional physical bonds are formed due to ionic complexation of fixed carboxyl groups with mobile metal ions.

Numerical analysis shows that the governing equations describe correctly experimental stress–strain diagrams, and material parameters change consistently with experimental conditions (maximum elongation ratio under stretching and minimum elongation ratio under retraction). The ability of the model to predict observations in multi-cycle tests with sophisticated deformation programs is confirmed by simulation, which reveals qualitative agreement with available experimental data.

An advantage of the model consists in (i) its simplicity for numerical implementation: as the governing relations involve differential equations only, no special procedures are required for solution of nonlinear integral equations (Long et al., 2014; Guo et al., 2016), (ii) the ability to determine material constants under one deformation program and to use them in order to predict the response in tests with another program (Figs. 6, 8 and 10), and (iii) high sensitivity of adjustable parameters to the physical mechanisms of non-covalent bonding (Tabs. 1 and 2).

Bearing in mind that cells growing on three-dimensional gel scaffolds can be considered as extra physical cross-links in a polymer network (Yang et al., 2017), the latter property provides an opportunity to evaluate the strength of their adhesion by comparing observations in mechanical tests on neat and cell-laden specimens. This issue will be discussed in detail in a subsequent study.

Acknowledgment

Financial support by the Innovation Fund Denmark (project 5152–00002B) is gratefully acknowledged.

Disclosure of interests

The authors declare no competing financial interest.

Appendix A.

Supplementary material.

References

Annabi, N.,Tamayol, A., Uquillas, J.A., Akbari, M., Bertassoni, L.E., Cha, C., Camci-Unal, G., Dokmeci, M.R., Peppas, N.A., Khademhosseini, A., 2014. Rational design and applications of hydrogels in regenerative medicine. Adv. Mater. 26, 85–124.

Bacca, M., Creton, C., McMeeking, R.M., 2017. A model for the Mullins effect in multinetwork elastomers. J. Appl. Mech. 84, 121009.

Bai, R., Yang, Q., Tang, J., Morelle, X.P., Vlassak, J., Suo, Z., 2017. Fatigue fracture of tough hydrogels. Extreme Mech. Lett. 15, 91–96.

Bergstrom, J.S., Boyce, M.C., 1998. Constitutive modeling of the large strain time-dependent behavior of elastomers. J. Mech. Phys. Solids 46, 931–954.

Brunelli, M., Perraulta, C.M., Lacroix, D., 2017. Short bursts of cyclic mechanical compression modulate tissue formation in a 3D hybrid scaffold. J. Mech. Behav. Biomed. Mater. 71, 165–174.

Cao, C., Li, L., Li, H., He, X., Wu, G., Yu, X., 2018. Cyclic biaxial tensile strain promotes bone marrow-derived mesenchymal stem cells to differentiate into cardiomyocyte-like cells by miRNA-27a. Int. J. Biochem. Cell Biol. 99, 125–132.

Charrier, E.E., Pogoda, K., Wells, R.G., Janmey, P.A., 2018. Control of cell morphology and differentiation by substrates with independently tunable elasticity and viscous dissipation. Nat. Comm. 9, 449.

Chaudhuri, O., Gu, L., Klumpers, D., Darnell, M., Bencherif, S.A., Weaver, J.C., Huebsch, N., Lee, H.-p., Lippens, E., Duda, G.N., Mooney, D.J., 2016. Hydrogels with tunable stress relaxation regulate stem cell fate and activity. Nat. Mater. 15, 326–334.

Chen, Q., Chen, H., Zhu, L., Zheng, J., 2016. Engineering of tough double network hydrogels. Macromol. Chem. Phys. 217 (2016) 1022–1036.

Chin, S.Y., Poh, Y.C., Kohler, A.-C., Compton, J.T., Hsu, L.L., Lau, K.M., Kim, S., Lee, B.W., Lee, F.Y., Sia, S.K., 2017. Additive manufacturing of hydrogel-based materials for next-generation implantable medical devices. Sci. Robotics 2, eaah6451.

Cooper, B.G., Stewart, R.C., Burstein, D., Snyder, B.D., Grinstaff, M.W., 2016. A tissue-penetrating double network restores the mechanical properties of degenerated articular cartilage. Angew. Chem. Int. Ed. 55, 4226–4230.

Creton, C., 2017. Networks and gels: Soft but dynamic and tough. Macromolecules 50, 8297–8316.

Cui, K., Sun, T.L., Kurokawa, T., Nakajima, T., Nonoyama, T., Chen, L., Gong, J.P., 2016. Stretching-induced ion complexation in physical polyampholyte hydrogels. Soft Matter 12, 8833–8840.

Dan, P., Velot, E., Decot, V., Menu, P., 2015. The role of mechanical stimuli in the vascular differentiation of mesenchymal stem cells. J. Cell Sci. 128, 2415–2422.

Dhote, D., Vernerey, F.J., 2014. Mathematical model of the role of degradation on matrix development in hydrogel scaffold. Biomech. Model. Mechanobiol. 13, 167–183.

Diani, J., Fayolle, B., Gilormini, P., 2009. A review on the Mullins effect. Eur. Polym. J. 45, 601–612.

Drozdov, A.D., 2010. Creep rupture and viscoelastoplasticity of polypropylene. Eng. Fract. Mech. 77, 2277–2293.

Drozdov, A.D., 2014. Self-oscillations of hydrogels driven by chemical reactions. Int. J. Appl. Mech. 6, 1450023.

Drozdov, A.D., 2017. Modeling the response of double-network gels with sacrificial junctions under swelling. Int. J. Solids Struct. 122–123, 175–188.

Drozdov, A.D., deClaville Christiansen, J., 2018. Nanocomposite gels with permanent and transient junctions under cyclic loading. Macromolecules 51, 1462–1473.

Drozdov, A.D., Gupta, R.K., 2003. Non-linear viscoelasticity and viscoplasticity of isotactic polypropylene. Int. J. Eng. Sci. 41, 2335–2361.

Drozdov, A.D., Klitkou, R., Christiansen, J.deC., 2013. Cyclic viscoplasticity of semicrystalline polymers with finite deformations. Mech. Mater. 56, 53–64.

Drozdov, A.D., Yuan, Q., 2003. The viscoelastic and viscoplastic behavior of low-density polyethylene. Int. J. Solids Struct. 40, 2321–2342.

Filippidi, E., Cristiani, T.R., Eisenbach, C.D., Waite, J.H., Israelachvili, J.N., Ahn, B.K., Valentine, M.T., 2017. Toughening elastomers using mussel-inspired iron-catechol complexes. Science 358, 502–505.

Fischenich, K.M., Lewis, J.T., Bailey, T.S., Haut Donahue, T.L., 2018. Mechanical viability of a thermoplastic elastomer hydrogel as a soft tissue replacement material. J. Mech. Behav. Biomed. Mater. 79, 341–347.

Frauchiger, D.A., Tekari, A., Woltje, M., Fortunato, G., Benneker, L.M., Gantenbein, B., 2017. A review of the application of reinforced hydrogels and silk as biomaterials for intervertebral disc repair. Eur. Cell Mater. 34, 271–290.

Gent, A.N., 1996. A new constitutive relation for rubber. Rubber Chem. Technol. 69, 59–61.

Green, M.S., Tobolsky, A.V., 1946. A new approach to the theory of relaxing polymeric media. J. Chem. Phys. 14, 80–92.

Gong, J.P., 2014. Materials both tough and soft. Science 344, 161–162.

Guo, J., Long, R., Mayumi, K., Hui, C.-Y., 2016. Mechanics of a dual cross-link gel with dynamic bonds: Steady state kinetics and large deformation effects. Macromolecules 49, 3497–3507.

Hao, J., Zhang, Y., Jing, D., Shen, Y., Tang, G., Huang, S., Zhao, Z., 2015. Mechanobiology of mesenchymal stem cells: Perspective into mechanical induction of MSC fate. Acta Biomater. 20, 1–9.

Hu, X., Zhou, J., Daniel, W.F.M., Vatankhah-Varnoosfaderani, M., Dobrynin, A.V., Sheiko, S.S., 2017. Dynamics of dual networks: Strain rate and temperature effects in hydrogels with reversible H-bonds. Macromolecules 50, 652–659.

Kitamura, N., Yokota, M., Kurokawa, T., Gong, J.P., Yasuda, K., 2016. In vivo cartilage regeneration induced by a double-network hydrogel: Evaluation of a novel therapeutic strategy for femoral articular cartilage defects in a sheep model. J. Biomed. Mater. Res. Part A 104, 2159- 2165.

Ko, H., Javey, A., 2017. Smart actuators and adhesives for reconfigurable matter. Acc. Chem. Res. 50, 691–702.

Leberfinger, A.N., Ravnic, D.J., Dhawan, A., Ozbolat, I.T., 2017. Concise review: Bioprinting of stem cells for transplantable tissue fabrication. Stem Cells Transl. Med. 6, 1940–1948.

Leijten, J., Seo, J., Yue, K., Trujillo-de Santiago, G., Tamayol, A., Ruiz-Esparza, G.U., Shin, S.R., Sharifi, R., Noshadi, I., Alvarez, M.M., Zhang, Y.S., Khademhosseini, A., 2017. Spatially and temporally controlled hydrogels for tissue engineering. Mater. Sci. Eng. R 119, 1–35.

Li, J., Mooney, D.J., 2016. Designing hydrogels for controlled drug delivery. Nat. Rev. Mater. 1, 16071.

Li, Y., Tang, S., Kroger, M., Liu, W.K., 2016. Molecular simulation guided constitutive modeling on finite strain viscoelasticity of elastomers. J. Mech. Phys. Solids 88, 204–226.

Liang, X., Deng, Y., Pei, X., Zhai, K., Xu, K., Tan, Y., Gong, X., Wang, P., 2017. Tough, rapid-recovery composite hydrogels fabricated via synergistic core shell microgel covalent bonding and Fe^{3+} coordination cross-linking. Soft Matter 13, 2654–2662.

Liu, Y., Zhang, H., Zheng, Y., 2016. A micromechanically based constitutive model for the inelastic and swelling behaviors in double network hydrogels. J. Appl. Mech. 83, 021008.

Liu, Y.-S., Liu, Y.-A., Huang, C.-J., Yen, M.-H., Tseng, C.-T., Chien, S., Lee, O.K., 2015. Mechanosensitive TRPM7 mediates shear stress and modulates osteogenic differentiation of mesenchymal stromal cells through Osterix pathway. Sci. Rep. 5, 16522.

Liu, Z., Tang, M., Zhao, J., Chai, R., Kang, J., 2018. Looking into the future: Toward advanced 3D biomaterials for stem-cell-based regenerative medicine. Adv. Mater. 30, 1705388.

Long, R., Mayumi, K., Creton, C., Narita, T., Hui, C.Y., 2014. Time dependent behavior of a dual cross-link self-healing gel: theory and experiments. Macromolecules 47, 7243–7250.

Lu, T., Wang, J., Yang, R., Wang, T.J., 2017. A constitutive model for soft materials incorporating viscoelasticity and Mullins effect. J. Appl. Mech. 84, 021010.

Luo, F., Sun, T.L., Nakajima, T., King, D.R., Kurokawa, T., Zhao, Y., Ihsan, A.B., Li, X., Guo, H., Gong, J.P., 2016. Strong and tough polyion-complex hydrogels from oppositely charged polyelectrolytes: A comparative study with polyampholyte hydrogels. Macromolecules 49, 2750–2760.

Mandrycky, C., Wang, Z., Kim, K., Kim, D.-H., 2016. 3D bioprinting for engineering complex tissues. Biotechnol. Adv. 34, 422–434.

Mann, J.L., Yu, A.C., Agmon, G., Appel, E.A., 2018. Supramolecular polymeric biomaterials. Biomater. Sci. 6, 10–37.

Mao, Y., Lin, S., Zhao, X., Anand, L., 2017. A large deformation viscoelastic model for double-network hydrogels. J. Mech. Phys. Solids 100, 103–130.

Meng, F., Pritchard, R.H., Terentjev, E.M., 2016. Stress relaxation, dynamics, and plasticity of transient polymer networks. Macromolecules 49, 2843–2852.

Nishida, T., Obayashi, A., Haraguchi, K., Shibayama, M., 2012. Stress relaxation and hysteresis of nanocomposite gel investigated by SAXS and SANS measurement. Polymer 53, 4533–4538.

Osada, Y., Gong, J.P., 1998. Soft and wet materials: Polymer gels. Adv. Mater. 10, 827–837.

Peppas, N.A., Van Blarcom, D.S., 2016. Hydrogel-based biosensors and sensing devices for drug delivery. J. Control. Release 240, 142–150.

Perez-San Vicente, A., Peroglio, M., Ernst, M., Casuso, P., Loinaz, I., Grande, H.-J., Alini, M., Eglin, D., Dupin, D., 2017. Self-healing dynamic hydrogel as injectable shock-absorbing artificial nucleus pulposus. Biomacromolecules 18, 2360–2370.

Rey-Rico, A., Cucchiarini, M., Madry, H., 2017. Hydrogels for precision meniscus tissue engineering: a comprehensive review. Connect. Tissue Res. 58, 317–328.

Rose, S., Dizeux, A., Narita, T., Hourdet, D., Marcellan, A., 2013. Time dependence of dissipative and recovery processes in nanohybrid hydrogels. Macromolecules 46, 4095–4104.

Song, Y., Tang, Y., Song, J., Lei, M., Liang, P., Fu, T., Su, X., Zhou, P., Yang, L., Huang, E., 2018. Cyclic mechanical stretch enhances BMP9-induced osteogenic differentiation of mesenchymal stem cells. Int. Orthop. 42, 947 955.

Tanaka, F., Edwards, S.F., 1992. Viscoelastic properties of physically cross-linked networks. Transient network theory. Macromolecules 25, 1516–1523.

Tanaka, Y., Kuwabara, R., Na, Y.-H., Kurokawa, T., Gong, J.P., Osada, Y., 2005. Determination of fracture energy of high strength double network hydrogels. J. Phys. Chem. B 109, 11559–11562.

Tang, J., Chen, X., Pei, Y., Fang, D., 2016. Pseudoelasticity and nonideal Mullins effect of nanocomposite hydrogels. J. Appl. Mech. 83, 111010.

Tang, Z., Chen, F., Chen, Q., Zhu, L., Yan, X., Chen, H., Ren, B., Yang, J., Qin, G., Zheng, J., 2017. The energy dissipation and Mullins effect of tough polymer/graphene oxide hybrid nanocomposite hydrogels. Polym. Chem. 8, 4659–4672.

Vernerey, F.J., Long, R., Brighenti, R., 2017. A statistically-based continuum theory for polymers with transient networks. J. Mech. Phys. Solids 107, 1–20.

Vernerey, F.J., 2018. Transient response of nonlinear polymer networks: A kinetic theory. J. Mech. Phys. Solids 115, 230–247.

Vining, K.H., Mooney, D.J., 2017. Mechanical forces direct stem cell behaviour in development and regeneration. Nat. Rev. Mol. Cell Biol. 18, 728–742.

Wang, Q., Gao, Z., 2016. A constitutive model of nanocomposite hydrogels with nanoparticle crosslinkers. J. Mech. Phys. Solids 94, 127–147.

Wang, W., Zhang, Y., Liu, W., 2017. Bioinspired fabrication of high strength hydrogels from non-covalent interactions. Progr. Polym. Sci. 71, 1–25.

Wojtecki, R.J., Meador, M.A., Rowan, S.J., 2011. Using the dynamic bond to access macroscopically responsive structurally dynamic polymers. Nat. Mater. 10, 14–27.

Yang, J., Zhang, Y.S., Yue, K., Khademhosseini, A., 2017. Cell-laden hydrogels for osteochondral and cartilage tissue engineering. Acta Biomater. 57, 1–25.

Yang, X., Liu, G., Peng, L., Guo, J., Tao, L., Yuan, J., Chang, C., Wei, Y., Zhang, L., 2017. Highly efficient self-healable and dual responsive cellulose-based hydrogels for controlled release and 3D cell culture. Adv. Funct. Mater. 27, 1703174.

Yu, Z., Liu, J., Tan, C.S.Y., Scherman, O.A., Abell, C., 2018. Supramolecular nested microbeads as building blocks for macroscopic self-healing scaffolds. Angew. Chem. Int. Ed. 57, 3079–3083.

Zhai, X., Ruan, C., Ma, Y., Cheng, D., Wu, M., Liu, W., Zhao, X., Pan, H., Lu, W.W., 2018. 3D-bioprinted osteoblast-laden nanocomposite hydrogel constructs with induced microenvironments promote cell viability, differentiation, and osteogenesis both in vitro and in vivo. Adv. Sci. 5, 1700550.

Zhang, L., Zhao, J., Zhu, J., Hea, C., Wang, H., 2012. Anisotropic tough poly(vinyl alcohol) hydrogels. Soft Matter 8, 10439–10447.

Zhang, W., Liu, X., Wang, J., Tang, J., Hu, J., Lu, T., Suo, Z., 2018. Fatigue of double-network hydrogels. Eng. Fracture Mech. 187, 74–93.

Zhao, X., 2014. Multi-scale multi-mechanism design of tough hydrogels: Building dissipation into stretchy networks. Soft Matter 10, 672–687.

Zhao, Y., Li, M., Liu, B., Xiang, J., Cui, Z., Qu, X., Qiu, D., Tian, Y., Yang, Z., 2018. Ultra-tough injectable cytocompatible hydrogel for 3D cell culture and cartilage repair. J. Mater. Chem. B 6, 1351–1358.

Zhou, J., Li, J., Du, X., Xu, B., 2017. Supramolecular biofunctional materials. Biomaterials 129, 1–27.

Zhou, J., Jiang, L., Khayat, R.E., 2018. A micro-macro constitutive model for finite-deformation viscoelasticity of elastomers with nonlinear viscosity. J. Mech. Phys. Solids 110, 137–154.

List of figures

Figure 1: Tensile stress σ versus elongation ratio λ. Symbols: experimental data on IH-gel (A) and H-gel (B) in loading–unloading tests with various $\lambda_{\rm max}$ (Liang et al., 2017). Solid lines: results of simulation.

Figure 2: Parameters P_{1*} and α versus the principal invariant $I_{\rm e2}$ at maximum elongation ratio $\lambda_{\rm max}$. Circles: treatment of observations in loading–unloading tests on IH-gel (A) and H-gel (B). Solid lines: results of simulation.

Figure 3: Tensile stress σ versus elongation ratio λ. Symbols: experimental data on IH-gel (A) and H-gel (B) in multi-cycle ($N = 4$) tests with various $\lambda_{{\rm max}\, n}$ and $\sigma_{\rm min} = 0$ (Liang et al., 2017). Solid lines: results of simulation.

Figure 4: Parameters P_{1*} and α versus the principal invariant $I_{\rm e2}$ at maximum elongation ratio $\lambda_{\rm max}$. Circles: treatment of observations in multi-cycle tests on IH-gel (A) and H-gel (B). Solid lines: results of simulation.

Figure 5: Parameter P_{2*} versus the principal invariant $I_{\rm i2}$ at minimum elongation ratio $\lambda_{\rm min}$. Circles: treatment of observations in multi-cycle tests on IH-gel (A) and H-gel (B). Solid lines: results of simulation.

Figure 6: Tensile stress σ versus elongation ratio λ. Circles: results of simulation for tensile tests. Solid lines: results of simulation for IH-gel (A,B) and H-gel (C,D) in multi-cycle tests with deformation programs (21) (A,C) and (22) (B,D).

Figure 7: Tensile stress σ versus elongation ratio λ. Solid lines: results of simulation for IH-gel (A) and H-gel (B) in multi-cycle ($N = 30$) tests with various maximum elongation ratios $\lambda_{\rm max}$ and minimum stress $\sigma_{\rm min} = 0$.

Figure 8: Maximum stress per cycle $\sigma_{\rm max}$ versus number of cycles n. Symbols: results of simulation for IH-gel (A) and H-gel (B) in multi-cycle ($N = 30$) tests with various maximum elongation ratios $\lambda_{\rm max}$ and minimum stress $\sigma_{\rm min} = 0$.

Figure 9: Tensile stress σ versus elongation ratio λ. Solid lines: results of simulation for IH-gel (A) and H-gel (B) in multi-cycle ($N = 30$) tests with various maximum stresses per cycle $\sigma_{\rm max}$ kPa and minimum stress $\sigma_{\rm min} = 0$.

Figure 10: Maximum elongation ratio per cycle $\lambda_{\rm max}$ versus number of cycles n. Symbols: results of simulation for IH-gel (A) and H-gel (B) in multi-cycle ($N = 30$) tests with various

maximum stresses per cycle σ_{max} kPa and minimum stress $\sigma_{\mathrm{min}} = 0$.

Tables

Table 1: Material parameters for DN gels (Fig. 1)

Parameter	IH-gel	H-gel
G (kPa)	30.2	22.0
K	90.0	65.0
a (s^{-1})	0.0	$6.4 \cdot 10^{-3}$
κ	0.3	0.21
γ_* (s^{-1})	0.09	0.09
Σ	4.0	0.8
α	0.0	
R_1	2.9	0.1

Table 2: Material parameters for DN gels (Fig. 3)

Parameter	IH-gel	H-gel
G (kPa)	28.2	21.4
K	180.0	65.0
a (s^{-1})	0.0	$6.7 \cdot 10^{-3}$
κ	0.4	0.21
γ_* (s^{-1})	0.09	0.09
Σ	4.0	0.8
α	0.0	
β (kPa^{-1})	35.0	35.0
R_1	2.9	0.1
R_2	$1.2 \cdot 10^4$	$1.5 \cdot 10^4$

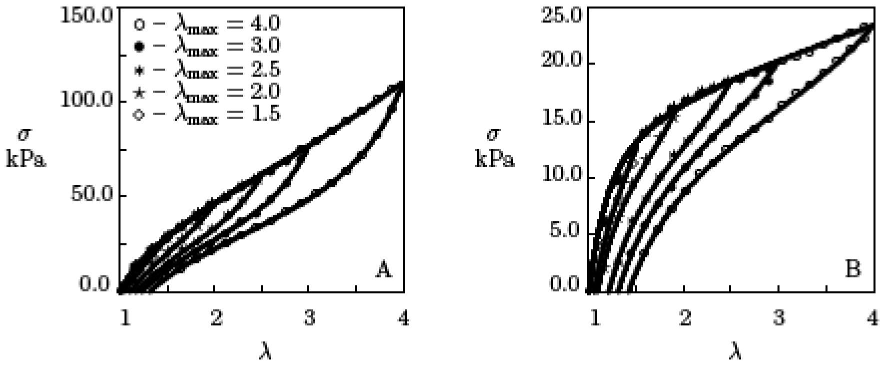
150.0
100.0
50.0
0.0
σ
kPa
○ − $\lambda_{\max} = 4.0$
● − $\lambda_{\max} = 3.0$
∗ − $\lambda_{\max} = 2.5$
★ − $\lambda_{\max} = 2.0$
◇ − $\lambda_{\max} = 1.5$
A
1
2
3
4
λ
25.0
20.0
15.0
10.0
5.0
0.0
σ
kPa
B
1
2
3
4
λ

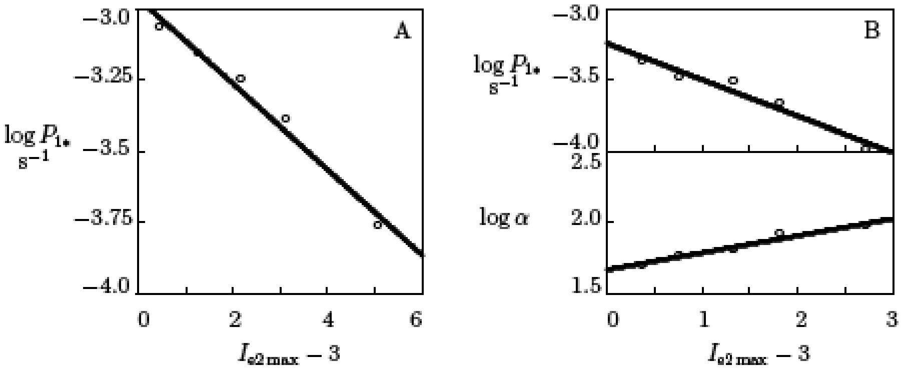
A
B
$\log P_{1*}$ s^{-1}
−3.0
−3.25
−3.5
−3.75
−4.0
0
2
4
6
$I_{e2\,max} - 3$
$\log P_{1*}$ s^{-1}
−3.0
−3.5
−4.0
2.5
2.0
1.5
$\log \alpha$
0
1
2
3
$I_{e2\,max} - 3$

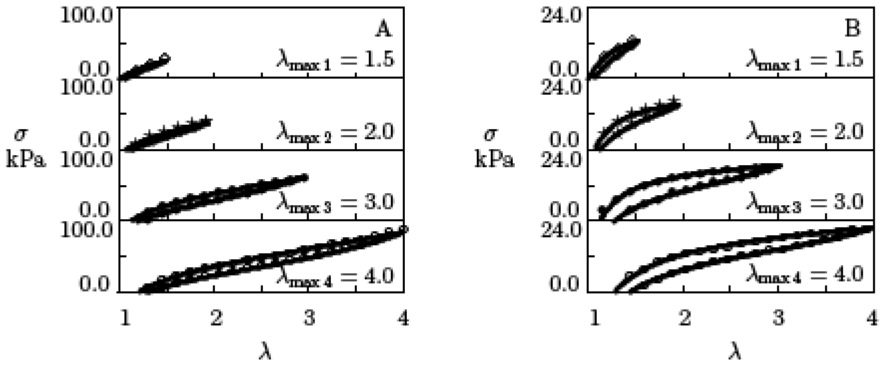
A
B
100.0
0.0
24.0
$\lambda_{\max 1} = 1.5$
$\lambda_{\max 2} = 2.0$
$\lambda_{\max 3} = 3.0$
$\lambda_{\max 4} = 4.0$
σ
kPa
1
2
3
4
λ

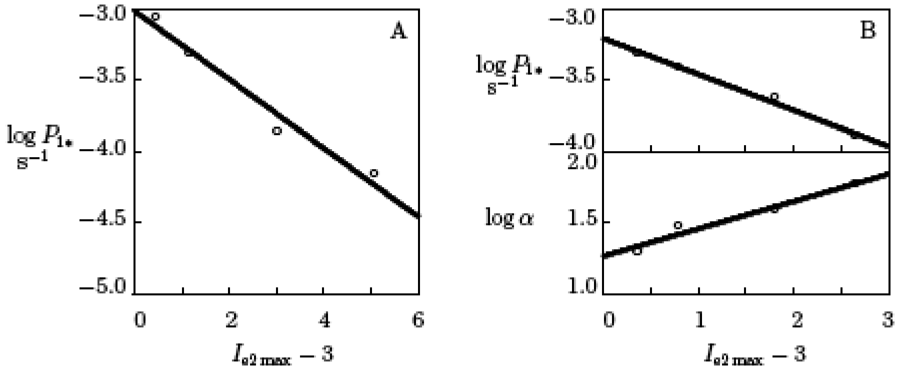
A
B
log P_{1*}
s^{-1}
−3.0
−3.5
−4.0
−4.5
−5.0
0
2
4
6
$I_{e2\,\max}-3$
log P_{1*}
s^{-1}
−3.0
−3.5
−4.0
log α
2.0
1.5
1.0
0
1
2
3
$I_{e2\,\max}-3$

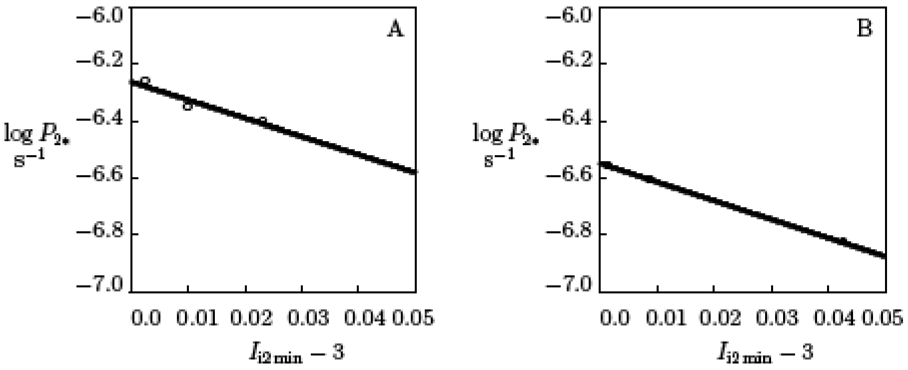
A
B
$\log P_{2*}$
s^{-1}
−6.0
−6.2
−6.4
−6.6
−6.8
−7.0
0.0
0.01
0.02
0.03
0.04
0.05
$I_{\mathrm{i2\,min}} - 3$

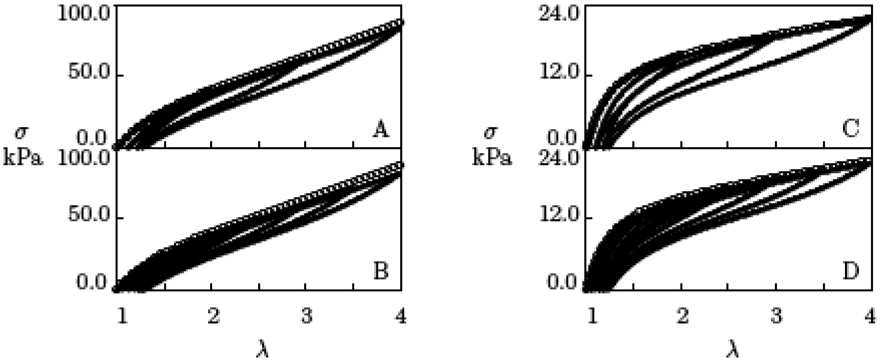
σ
kPa
100.0
50.0
0.0
A
100.0
50.0
0.0
B
1
2
3
4
λ
σ
kPa
24.0
12.0
0.0
C
24.0
12.0
0.0
D
1
2
3
4
λ

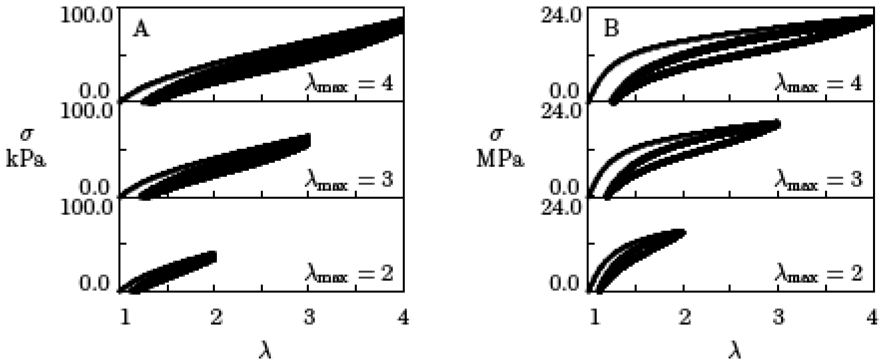
A
B
σ
kPa
σ
MPa
100.0
0.0
24.0
$\lambda_{\max} = 4$
$\lambda_{\max} = 3$
$\lambda_{\max} = 2$
1
2
3
4
λ

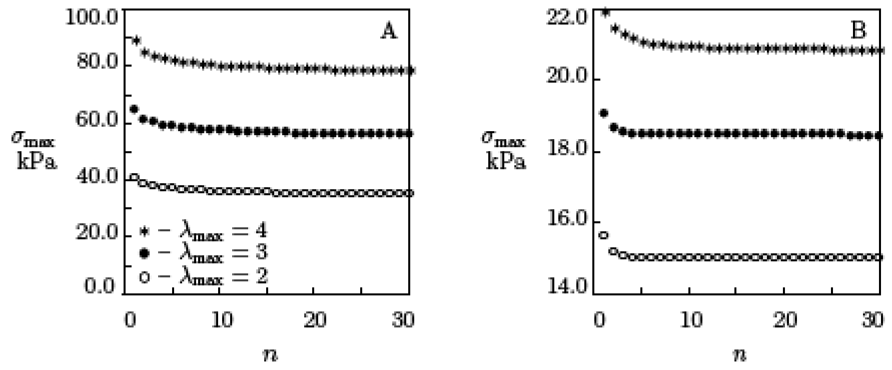
A
$\sigma_{\max}$ kPa
100.0
80.0
60.0
40.0
20.0
0.0
0
10
20
30
n
$* - \lambda_{\max} = 4$
$\bullet - \lambda_{\max} = 3$
$\circ - \lambda_{\max} = 2$
B
$\sigma_{\max}$ kPa
22.0
20.0
18.0
16.0
14.0
0
10
20
30
n

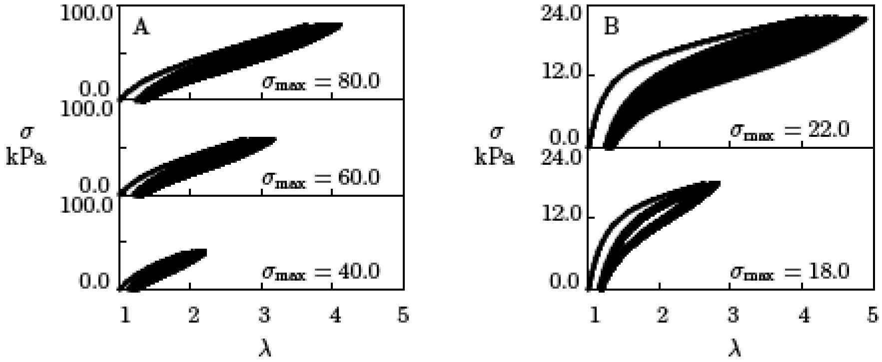
A
100.0
0.0
$\sigma_{\max} = 80.0$
100.0
0.0
$\sigma_{\max} = 60.0$
100.0
0.0
$\sigma_{\max} = 40.0$
σ
kPa
1
2
3
4
5
λ
B
24.0
12.0
0.0
$\sigma_{\max} = 22.0$
24.0
12.0
0.0
$\sigma_{\max} = 18.0$
σ
kPa
1
2
3
4
5
λ

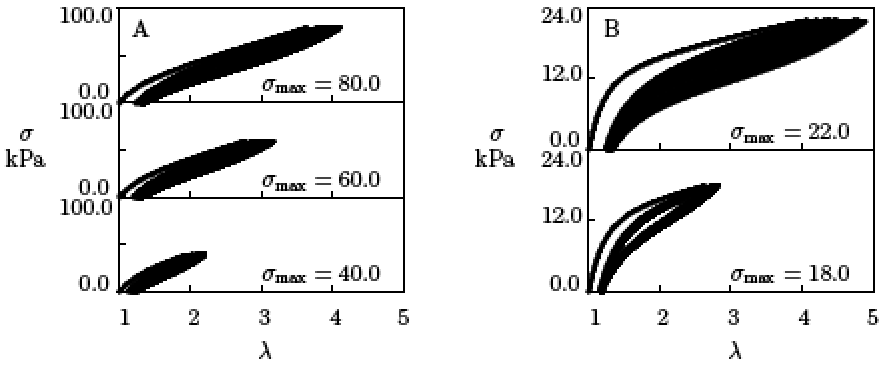
A
100.0
0.0
$\sigma_{\max} = 80.0$
100.0
0.0
$\sigma_{\max} = 60.0$
100.0
0.0
$\sigma_{\max} = 40.0$
σ
kPa
1
2
3
4
5
λ
B
24.0
12.0
0.0
$\sigma_{\max} = 22.0$
24.0
12.0
0.0
$\sigma_{\max} = 18.0$
σ
kPa
1
2
3
4
5
λ

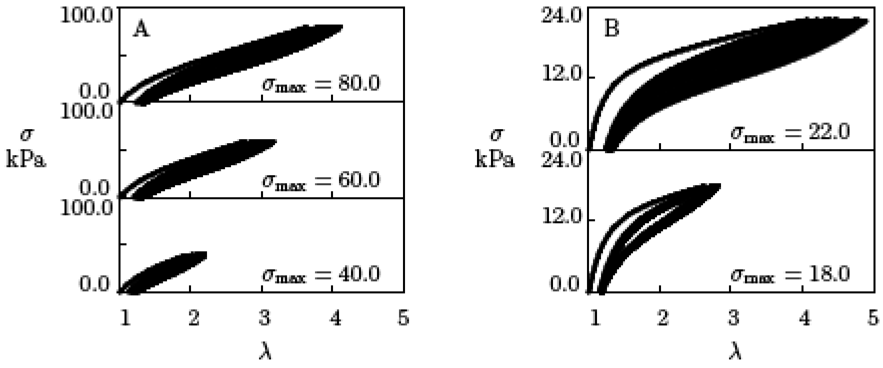
A
100.0
0.0
$\sigma_{\max} = 80.0$
100.0
0.0
$\sigma_{\max} = 60.0$
100.0
0.0
$\sigma_{\max} = 40.0$
σ
kPa
1
2
3
4
5
λ
B
24.0
12.0
0.0
$\sigma_{\max} = 22.0$
24.0
12.0
0.0
$\sigma_{\max} = 18.0$
σ
kPa
1
2
3
4
5
λ

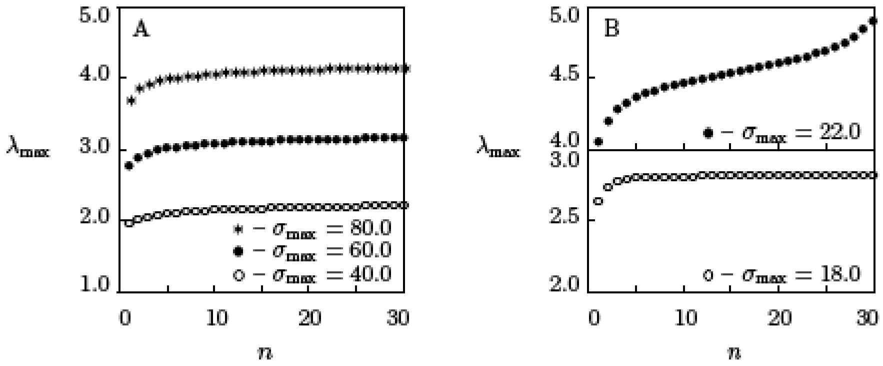
A
$\lambda_{\max}$
5.0
4.0
3.0
2.0
1.0
0
10
20
30
n
* – $\sigma_{\max} = 80.0$
● – $\sigma_{\max} = 60.0$
○ – $\sigma_{\max} = 40.0$
B
$\lambda_{\max}$
5.0
4.5
4.0
3.0
2.5
2.0
0
10
20
30
n
● – $\sigma_{\max} = 22.0$
○ – $\sigma_{\max} = 18.0$